Article

Chemistry & Biology

Toward the Rational Design of Carbapenem Uptake in *Pseudomonas aeruginosa*

Graphical Abstract

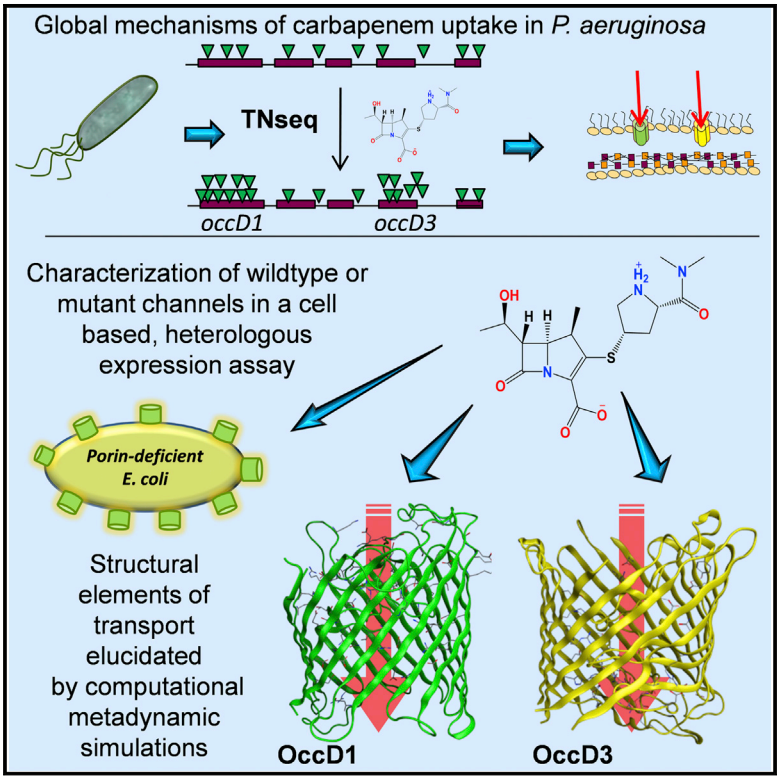

Highlights

- TNseq is used to discover novel carbapenem uptake mechanisms
- Pseudomonal porin OccD3 is involved in carbapenem uptake
- Metadynamics simulations describe carbapenem uptake on an atomic scale
- Rational carbapenem design and synthesis lead to altered uptake properties

Authors

Vincent M. Isabella, Arthur J. Campbell, ..., Ruben Tommasi, Alita A. Miller

Correspondence

alita.miller@astrazeneca.com (A.A.M.), ruben.tommasi@astrazeneca.com (R.T.)

In Brief

Isabella et al. utilize a multidisciplinary approach including genetics, molecular dynamics simulations, and medicinal chemistry to probe carbapenem uptake by *Pseudomonas aeruginosa.* A novel uptake mechanism was discovered and novel carbapenems with altered uptake properties were synthesized and characterized.

Isabella et al., 2015, Chemistry & Biology *22*, 535–547
April 23, 2015
http://dx.doi.org/10.1016/j.chembiol.2015.03.018

CellPress

Chemistry & Biology
Article

Toward the Rational Design of Carbapenem Uptake in *Pseudomonas aeruginosa*

Vincent M. Isabella,[1] Arthur J. Campbell,[2] John Manchester,[3] Mark Sylvester,[3] Asha S. Nayar,[3] Keith E. Ferguson,[3] Ruben Tommasi,[3,*] and Alita A. Miller[3,*]
[1]Synlogic, 25 First Street, Cambridge, MA 02141, USA
[2]Stanley Center for Psychiatric Research, Broad Institute of Massachusetts Institute of Technology and Harvard University, 415 Main Street, Cambridge, MA 02142, USA
[3]AstraZeneca Infection Innovative Medicines, 35 Gatehouse Drive, Waltham, MA 02451, USA
*Correspondence: alita.miller@astrazeneca.com (A.A.M.), ruben.tommasi@astrazeneca.com (R.T.)
http://dx.doi.org/10.1016/j.chembiol.2015.03.018

SUMMARY

Understanding how compound penetration occurs across the complex cell walls of Gram-negative bacteria is one of the greatest challenges in discovering new drugs to treat the infections they cause. A combination of next-generation transposon sequencing, computational metadynamics simulations (CMDS), and medicinal chemistry was used to define genetic and structural elements involved in facilitated carbapenem entry into *Pseudomonas aeruginosa*. Here we show for the first time that these compounds are taken up not only by the major outer membrane channel OccD1 (also called OprD or PA0958) but also by a closely related channel OccD3 (OpdP or PA4501). Transport-mediating molecular interactions predicted by CMDS for these channels were first confirmed genetically, then used to guide the design of carbapenem analogs with altered uptake properties. These results bring us closer to the rational design of channel transmissibility and may ultimately lead to improved permeability of compounds across bacterial outer membranes.

INTRODUCTION

Limited classes of antibiotics are available to treat *Pseudomonas aeruginosa* infections due to both intrinsic and acquired resistance determinants, which include alterations in membrane permeability, enhanced mechanisms of multi-drug efflux, and acquisition of β-lactamases (Breidenstein et al., 2011). Increasing antibiotic resistance in *P. aeruginosa* has led to major concerns about the ability to successfully treat infections caused by this important opportunistic pathogen (Fraimow and Nahra, 2013; Pendleton et al., 2013). The carbapenems are an important class of antibiotics that remain in use for *P. aeruginosa* infections as they are less prone to degradation by extended spectrum β-lactamases (Papp-Wallace et al., 2011). Nevertheless, emerging carbapenem resistance is on the rise; therefore the clinical utility of this class may also dwindle in the near future.

One of the biggest challenges in the design and development of new drugs for the treatment of infections caused by *P. aeruginosa* and other serious Gram-negative pathogens is our relative ignorance of the molecular mechanisms driving compound penetration across their outer membranes. One of the most notable features of *P. aeruginosa* is its low outer membrane permeability, which has been estimated to be only ~8% of other bacterial membranes such as that of *Escherichia coli* (Hancock and Woodruff, 1988). Unlike *E. coli*, which contain several large and relatively nonspecific general porins, *P. aeruginosa* deploys a variety of specialized outer membrane proteins to facilitate uptake of nutrients needed for growth and survival (Hancock and Brinkman, 2002), some of which are nonspecific channels, such as OprF, and others that are substrate-specific transporters with small pores, such as the Occ (outer membrane carboxylate channel) family of transporters (Eren et al., 2012), also known as the OprD family of channels (Tamber et al., 2006). The 19 members in the latter family have been further classified according to their preferential substrate selectivity; although all family members prefer their substrates to contain carboxylates, the OccD subfamily prefers cations (Liu et al., 2012b) while the OccK subfamily takes up anions (Liu et al., 2012a). This classification is based on data generated by fairly cumbersome techniques such as liposome swelling assays (Hajjar et al., 2010), doubling time experiments (Tamber et al., 2006), or radiolabeled substrate competition assays using membrane vesicles containing individually overexpressed channels (Eren et al., 2013, 2012). These challenging assays underscore an additional need for this field of study, namely the development of robust methods to more precisely assess compound uptake.

OccD1 (also called OprD or PA0958), the first member of the Occ family to be characterized in depth, transports basic amino acids (Figure 1, compounds **1** and **2**) and, fortuitously, also facilitates entry of certain privileged carbapenems such as meropenem and imipenem (Figure 1, compounds **4** and **5**). Indeed, the first documented case of clinical resistance to this class of antibiotics in *P. aeruginosa* was found to be due to loss of this outer membrane protein (Quinn et al., 1986), and it is now well established that changes in OccD1 expression levels or sequence are frequently associated with resistance to carbapenems in the clinic (Quale et al., 2006), (Pirnay et al., 2002). A recent crystal structure of OccD1 (PDB 3SY7) (Eren et al., 2012), (Biswas et al., 2007) revealed an 18-strand β-barrel containing a small channel lined on one side with a positively charged basic amino

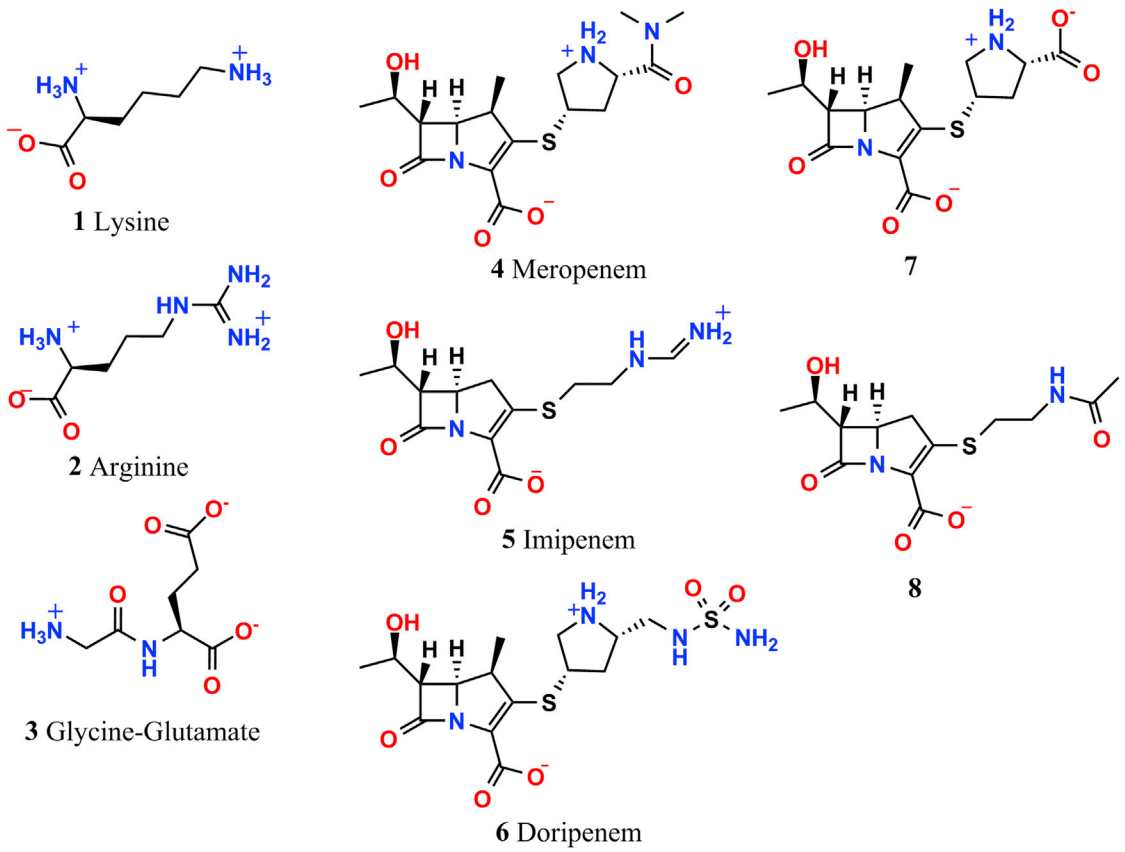

Figure 1. Structures of Compounds Studied in this Work

1, Lysine; **2**, arginine; **3**, glycine-glutamate dipeptide; **4**, meropenem; **5**, imipenem; **6**, doripenem; **7**, meropenem analog 7; **8**, imipenem analog 8.

acid ladder. This is often called the constriction zone and is widely accepted as the place where nutrients, ions, substrates, and/or water pass through from the extracellular to the periplasmic space. The structure also revealed that the L7 insertion loop (L7i) and the L3 loop within the protein, which abut the constriction zone, may play a role in recognition of natural substrates (Figure 2B) (Eren et al., 2012). The L7 loop forms a crown of backbone carbonyls that are separated approximately 120° relative to the basic ladder. This feature creates an electrostatic recognition framework that has a handedness ideally selective for the zwitterionic backbone amine and carboxylic acid of a free α-amino acid. It is not immediately clear how OccD1 selects for the basic side chains of the basic amino acids but it is reasonable to postulate that the electronegative recognition pocket of OccD1 may play a role. The interactions that occur during translocation through the constriction zone likely dictate the selectivity of the channels and therefore the constriction zone is one of the most important regions to study to better understand the molecular recognition of this transporter. The diameter of the constriction zone based on the crystallographic structure is ~6 Å (between the backbone carbonyl oxygens of Q304 and G128, the closest pair of atoms in OccD1) and has a length of ~15 Å (A318 to H395 Cα-Cα distance). This small constriction zone coupled with electrophysiology experiments led van den Berg and colleagues to suggest that the structure is most likely in a closed state (Eren et al., 2012). They subsequently tested a series of amino acid substitutions to examine the role of specific residues predicted to be involved in arginine uptake (Eren et al., 2012); a subset of these are described in more detail below.

Given the likelihood that the structural features shared between the natural substrates of OccD1 and the carbapenems serve as the molecular basis of their uptake, it is possible that an improved understanding of how the recognition events of the natural substrates occur could lead to the design of carbapenems with enhanced uptake properties. In addition, it may eventually be possible to design compounds that enter simultaneously through multiple channels. These may have a decreased risk for emergence of clinical resistance, since multiple channel mutations would need to arise simultaneously for resistance to occur. Ultimately, the ability to predict the uptake by different channels may enable rational design of molecules with enhanced uptake properties that may translate into more efficacious antibiotics, which are so desperately needed.

To that end, we utilized a multidisciplinary approach to begin addressing this challenging problem. In the first part of this study, we characterized the uptake of meropenem by *P. aeruginosa* on a global scale through the use of next-generation transposon junction sequencing (TNseq). This relatively new platform allows for a snapshot of the contribution of all potential outer membrane transporters to drug susceptibility during a

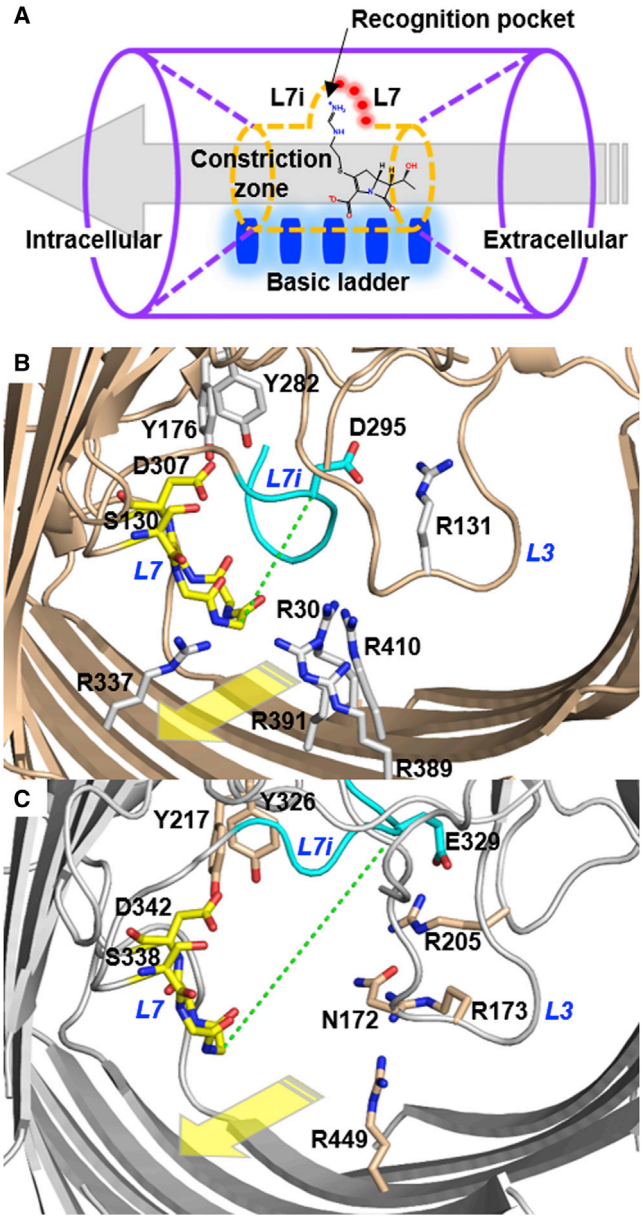

Figure 2. Structural Overview of OccD1 and OccD3

(A) Schematic view showing the main substrate recognition elements in the porins. Residues are labeled according to OccD1. From the extracellular vestibule, the substrate first encounters residues of the basic ladder (blue rectangles) and then enters the recognition pocket formed between the L7 and L7i loops, where it interacts with D307 (D342), as well as the crown of carbonyls in the L7 loop (shown as red dots), while retaining interactions with the basic ladder. From there, the substrate moves through the constriction zone and into the periplasmic space.

(B and C) Cartoon representations of a substrate-specific recognition pocket of OccD1 and OccD3, respectively. Images of OccD1 and OccD3 were created using PyMOL and generated from PDB IDs 3SY7 and 3SYB, respectively. (B) Side view of OccD1. (C) Side view of OccD3. The N-terminal sequence PAPDNPSYAAEVQSIPSV of OccD3 was removed for clarity. Dashed lines in green represent measured distances of 8.3 Å and 15.7 Å, which correlate between C_α carbons of D295 and Q304 and Q329 and L340 for OccD1 and OccD3, respectively. Arrows represent extracellular to periplasmic space direction.

course of exposure and led to the identification of a second OccD subfamily channel, OccD3 (OpdP or PA4501), which is also capable of transporting carbapenems. The second component of this study was inspired by recent efforts of Ceccarelli and colleagues to build an understanding of channel function in several species of Gram-negative bacteria using molecular dynamic simulation (Hajjar et al., 2010; Kumar et al., 2010). Recently, a similar study exploring translocation of arginine in OccD1 was published by Parkin and Khalid (2014). Our approach used molecular metadynamics simulations, an atomistic simulation technique that provides information about dynamical processes at atomic resolution (Laio and Parrinello, 2002), to study compound permeation through OccD1 and OccD3. Unlike traditional molecular dynamics methods, this allows the input of small amounts of energy to a system to enhance the sampling of physiologically interesting processes such as the translocation of small molecules through the OccD channels. Subtracting the applied potential energy from the final simulation provides a free energy profile for the process of interest. Using this approach, in addition to confirming the role of OccD1 in meropenem uptake, we found that the lowest-energy path for translocation of imipenem mimics that of the natural substrate arginine in OccD1. Interestingly, while meropenem does not appear to bind deeply in the pocket in our simulations, it does make contact with the backbone carbonyls of the L7 loop, which are part of the recognition pocket. Furthermore, simulations on OccD3 predict that imipenem and meropenem mimic the pathway for its natural dipeptide substrate glycine-glutamate (Gly-Glu) (Figure 1, compound **3**). The third aspect of our approach involved synthesizing carbapenem analogs to chemically probe some of the required features of permeation while seeking to maintain the inherent acylation activity of the penicillin binding protein (PBP) enzymes intact. We were able to generate an analog of meropenem for which a simple substitution on the side chain resulted in diminished dependence on OccD1 for translocation, an important discovery that could lead to better understanding of the design of improved carbapenems addressing *P. aeruginosa* resistance. Finally, using an imipenem analog, we demonstrated that alteration of the basic side chain results in complete ablation of antibacterial activity that is solely driven by permeation effects (as enzymatic activity is actually improved over the parent structure). The deployment of such a multidisciplinary approach to study the factors influencing drug permeation may represent a breakthrough in the ability to design compounds with enhanced outer membrane permeability, one of the greatest barriers in the development of effective antibacterial drugs.

RESULTS

TNseq Confirms the Primary Role of OccD1 in Meropenem Uptake

The channel OccD1 plays an important role in carbapenem uptake in *P. aeruginosa*; its inactivation results in a 4- to 8-fold decrease in meropenem susceptibility against laboratory strains (Köhler et al., 1999). We used TNseq to both confirm the primary role of OccD1 in meropenem uptake and validate this method for the determination of bacterial drug uptake mechanisms in general. TNseq, or high throughput transposon junction sequencing of saturated mutant libraries, is a recently developed platform

Table 1. Nonessential Genes whose Inactivation Confers Meropenem Resistance in Wild-Type versus *occD1*, also called *oprD*, Mutant Strains of PAO1

LOCUS ID	Gene Name	Function	Cellular Location	Fold Enrichment
Wild-Type PAO1				
PA0958	occD1/oprD	small molecule transport	outer membrane	71.6
PA3574	nalD	regulator of efflux	cytoplasm	60.01
PA1796	folD	folate metabolism	cytoplasm	59.86
PA0424	mexR	regulator of efflux	cytoplasm	41.15
PA5027	PA5027	hypothetical	cytoplasm	40.04
PA3721	nalC	regulator of efflux	cytoplasm	37.94
PA3967	PA3967	hypothetical	cytoplasm	25.25
PA2810	copS	phosphorelay sensor kinase	inner membrane	23.87
PA3831	pepA	leucine aminopeptidase	cytoplasm	21.19
PA0890	aotM	arginine/ornithine transport	inner membrane	21.07
PA5244	PA5244	hypothetical	inner membrane	18.18
PA0161	PA0161	hypothetical	unknown	17.7
PA2620	clpA	ATP-binding protease	cytoplasm	17.24
PA4076	PA4076	hypothetical	inner membrane	17.1
PA5548	PA5548	probable transporter	inner membrane	16.24
PA5333	PA5333	hypothetical	inner membrane	15.96
PA0358	PA0358	hypothetical	unknown	15.04
PA4218	ampP	siderophore transport	inner membrane	14.44
PA4000	rplA	rare lipoprotein A homolog	unknown	13.7
PA0571	PA0571	hypothetical	unknown	12.84
PA3674	PA3674	hypothetical	unknown	12.69
PA4522	ampD	regulator of ampC	cytoplasm	12.63
PA0467	PA0467	hypothetical	unknown	11.86
PA4896	PA4896	probable sigma factor	cytoplasm	11.15
PA5086	PA5086	hypothetical	unknown	10.96
ΔoccD1 PAO1				
PA3453	PA3453	hypothetical	unknown	235.79
PA3902	PA3902	hypothetical	periplasm	219.23
PA4181	PA4181	hypothetical	unknown	211.05
PA5419	soxG	sarcosine catabolism	cytoplasm	206.47
PA3721	nalC	regulator of transport	regulator of efflux	202.4
PA4160	fepD	enterobactin transporter	inner membrane	192.29
PA1180	phoQ	phosphorelay sensor kinase	inner membrane	106.72
PA3574	nalD	regulator of transport	regulator of efflux	106.13
PA4522	ampD	regulator of ampC	cytoplasm	101.84
PA0424	mexR	regulator of efflux	cytoplasm	90.76
PA0468	PA0468	hypothetical	unknown	60.81
PA0084	tssC1	type VI secretion system	cytoplasm	59.57
PA4501	occD3/opdP	Glyc-Glu dipeptide porin	outer membrane	47.57
PA5443	uvrD	DNA helicase (stress response)	cytoplasm	46.45
PA4020	mpl	UDP-N-acetylmuramate-alanine ligase	cytoplasm	43.07
PA1121	yfiR	hypothetical	periplasm	42.06
PA3019	PA3019	ATP-binding subunit of ABC transporter	cytoplasm	38.37
PA4058	PA4058	hypothetical	unknown	37.16
PA4506	PA4506	ATP-binding subunit of ABC transporter	cytoplasm	36.23
PA4726	cbrB	phosphorelay response regulator	cytoplasm	34.21
PA4799	PA4799	hypothetical	unknown	26.91

(*Continued on next page*)

Table 1. *Continued*

LOCUS ID	Gene Name	Function	Cellular Location	Fold Enrichment
PA4001	sltB1	soluble lytic transglycosylase B	inner membrane	24.55
PA3831	pepA	leucine aminopeptidase	cytoplasm	23.76
PA4725	cbrA	phosphorelay sensor kinase	inner membrane	22.66
PA0545	PA0545	hypothetical	inner membrane	20.55

The locus ID, gene name and function, and cellular location of the top 15 genes whose inactivation resulted in the highest levels of enrichment after drug treatment are shown.

(van Opijnen et al., 2014) that is currently being used to evaluate fitness and/or virulence determinants in a wide variety of bacterial pathogens (see for example Subashchandrabose et al., 2013; Palace et al., 2014; Wang et al., 2014), including *P. aeruginosa* (Skurnik et al., 2013). A pool of approximately 50,000 unique transposon insertion mutants in PA01 was exposed to meropenem at 1× minimum inhibitory concentration (MIC) in rich media for 6 hr, at which point the surviving cells were collected for TNseq analysis. As expected, a number of mutants with previously described roles in carbapenem resistance, such as negative regulators of efflux (*mexR*, *nalD*, and *nalC*) or β-lactamase activity (*ampD*) (Moya et al., 2009; Sobel et al., 2005), were found to be highly enriched in the meropenem-treated sample (Table 1, upper panel). Mutants with transposon insertions in *occD1* were also found to be greatly enriched, confirming the previously established role of OccD1 in the uptake of this compound. No other genes encoding outer membrane proteins showed this degree of enrichment (Table S1). These data suggest that that no additional channels contribute significantly to meropenem uptake by *P. aeruginosa* in rich media when OccD1 is present. Representative single transposon mutants from those found to be most highly enriched by this selection were tested individually for relative sensitivity to meropenem by disk diffusion on both rich and minimal media (data not shown); all those tested were found to be less susceptible than the wild-type parent PAO1, confirming our TNseq results and validating the platform.

TNseq Analysis Reveals an Additional Mechanism of Meropenem Uptake

Although an *occD1* deletion mutation in PAO1 results in an elevated meropenem MIC (Köhler et al., 1999), this concentration is at or near the CLSI breakpoint of 2 μg/ml (Hombach et al., 2012). The fact that meropenem still shows some activity in an *occD1* deletion mutant suggests that alternative mechanisms of meropenem uptake exist in the absence of functional OccD1. In order to test this hypothesis, we constructed a transposon mutant library (also containing ~50,000 unique insertions) in a PAO1 *ΔoccD1* background and subjected this second pooled library to meropenem stress in the same manner as the wild-type parent. Again, mutations in genes involved in repression of efflux and β-lactamases were found to be highly enriched, as expected (Table 1, lower panel). Of particular note was the significant enrichment of TN mutations in *occD3* (PA4501; Table S1). OccD3 is another member of the OccD subfamily of channels in *P. aeruginosa* that bears the highest degree (50%) of homology to OccD1 (Tamber and Hancock, 2006). Although this transporter preferentially allows uptake of glycine-glutamate dipeptides (Tamber et al., 2006), it has been shown that it, like OccD1, is also capable of transporting arginine and that its expression is specifically upregulated upon arginine exposure (Tamber and Hancock, 2006). This redundancy in function between OccD1 and OccD3 combined with our TNseq results strongly suggested that OccD3 may constitute a secondary carbapenem uptake mechanism.

The Loss of occD3 Causes a Significant Increase in Carbapenem MIC when Combined with Loss of occD1

To confirm the relative contribution of OccD1 and OccD3 in carbapenem uptake as suggested by the TNseq results, deletions of both genes, alone and in combination, were generated in a PAO1 background, and MICs of these mutant strains were determined in rich (MHBII) and minimal (M9S) media. As summarized in Table 2, inactivation of *occD1* resulted in a 4-fold increase in MIC for the carbapenems (meropenem, imipenem, and doripenem) in rich medium, with no changes in susceptibility observed for control compounds (ceftazidime, tobramycin, and ofloxacin). Inactivation of *occD3* alone did not result in a significant change in susceptibility to any compound tested in either rich or minimal medium. Although the MIC of the carbapenems was significantly lower in minimal medium for all the strains tested, only a 2-fold difference was observed for the wild-type versus the *occD1* mutant under these conditions. However, a *ΔoccD1ΔoccD3* double mutant led to a remarkable decrease in susceptibility to the carbapenems (16- to 64-fold) but not control compounds. A decrease in susceptibility, albeit less striking, was also observed when the same comparison was made in rich medium (4- to 16-fold). Expression of OccD1 or OccD3 in the *ΔoccD1ΔoccD3* double mutant *in trans* restored susceptibility to carbapenems and led to lower MICs than observed for the wild-type parent, whereas no effect was seen for control compounds or when a member of the OccK subfamily (OccK7, also called OpdD) was overexpressed. These results clearly demonstrate that both OccD1 and OccD3 specifically facilitate the transport of carbapenems and suggest that both channels may do so concomitantly under nutrient limiting conditions. Results for control compounds confirmed that the effect of channel overexpression was channel specific, and did not cause a general increase in the porosity of the outer membrane. To determine if other closely related OccD subfamily members also play a role in carbapenem uptake, a strain was generated with deletions in the genes encoding the five OccD channels with the greatest level of expression based on RNA seq analysis of PAO1 in minimal medium (data not shown), namely *ΔoccD1*, *ΔoccD2* (*ΔopdC*), *ΔoccD3*, *ΔoccD4* (*ΔopdT*), and *ΔoccD7* (*ΔopdB*). No difference in susceptibility was observed between the

Table 2. Genetic Confirmation that Carbapenem Transport Is Facilitated by OccD1 and OccD3

	MER	Fold Change[a]	IMP	Fold Change[a]	DOR	Fold Change[a]	Compound **7**	Fold Change[a]	CAZ	TO	OX
Rich medium (MHBII)											
PAO1	0.5	–	1	–	1	–	4	–	2	0.5	0.5
ΔoccD1	2	↑4×	8	↑8×	2	↑2×	8	↑2×	2	0.5	0.5
ΔoccD3	1	↑2×	1	NC	1	NC	4	NC	2	1	0.5
ΔoccD1 ΔoccD3	4	↑8×	16	↑16×	4	↑4×	8	↑2×	2	0.5	0.5
ΔoccD1-occD4, ΔoccD7	4	↑8×	16	↑16×	4	↑4×	8	↑2×	2	0.5	1
ΔoccD1 ΔoccD3/pPSV35 (empty)	4	–	16	–	2	–	4	–	1	0.5	0.5
ΔoccD1 ΔoccD3/pPSV35_occD1	0.125	↓32×	0.25	↓64×	0.125	↓16×	2	↓2×	1	1	0.5
ΔoccD1 ΔoccD3/pPSV35_occD3	0.25	↓16×	0.5	↓32×	0.25	↓8×	2	↓2×	1	1	0.5
ΔoccD1 ΔoccD3/pPSV35_occK7	4	NC	16	NC	2	NC	4	NC	1	1	0.5
Minimal media (M9S)											
PAO1	0.031	–	0.25	–	0.063	–	0.25	–	1	2	0.5
ΔoccD1	0.063	↑2×	0.5	↑2×	0.125	↑2×	0.5	↑2×	2	2	0.5
ΔoccD3	0.031	NC	0.25	NC	0.063	NC	0.25	NC	2	1	0.5
ΔoccD1 ΔoccD3	2	↑64×	4	↑16×	1	↑16×	0.5	↑2×	2	1	0.5
ΔoccD1-occD4, ΔoccD7	2	↑64×	4	↑16×	1	↑16×	0.5	↑2×	1	1	0.5

The activity (MIC, in μg/ml) of each test compound against PAO1 wild-type versus channel-deficient strains in the absence and presence of complementing plasmids in rich (MHBII) versus minimal (M9S) medium is shown. Where indicated, fold change is relative to the activity of the PAO1 parent strain. MER, meropenem; IMP, imipenem; DOR, doripenem; CAZ, ceftazidime; TO, tobramycin; OX, ofloxacin. All MIC tests were performed at least in triplicate.

[a]Compared with activity against parent PAO1.

five-channel mutant and the *ΔoccD1ΔoccD3* double mutant in either medium tested (Table 2), suggesting that only OccD1 and OccD3 are major contributors to carbapenem transport under these conditions.

Characterization of Transporters in a Cell-Based Heterologous Expression Assay

P. aeruginosa contains 19 outer membrane channels in the OccD and OccK subfamilies that are highly similar to one another and whose expression is controlled by complex regulatory pathways. This complexity is further confounded by numerous efflux systems, which limits our ability to analyze the relative contribution of individual channels in carbapenem uptake in a *P. aeruginosa* background beyond the broad conclusions made above. Therefore, to further examine the function of OccD1 and OccD3 in carbapenem uptake, we developed a cell-based assay that relies on the heterologous expression of these channels in *E. coli* Omp8 (Prilipov et al., 1998). Genes encoding all the major endogenous *E. coli* porins (namely *lamB, ompF*, *ompA*, and *ompC*) have been deleted in this strain. As shown in Table 3, expression of OccD1 or OccD3 in Omp8 in trans caused a 32-fold and 16-fold decrease in the MIC of meropenem, respectively, whereas expression of another member of the OccD subfamily, OccD2 (or OpdC [PA0162]), or of an OccK subfamily channel, OccK7 (or OpdD [PA1025]), had little to no effect. Similar MIC patterns were also observed for imipenem and doripenem against these strains, whereas the activity of control compounds (ceftazidime, tobramycin, and ofloxacin) were unaffected (Table 3).

The ability of carbapenems to compete with the natural substrates of the OccD1 and OccD3 channels was also explored. We found that 50 mM concentrations of arginine and lysine, but not glycine-glutamate (Gly-Glu), reduced the activity of meropenem in *E. coli* Omp8 overexpressing OccD1 but had no effect on OccD3-overexpressing strains (Table 4). However, no significant effect was observed upon competition with imipenem under any of the conditions tested. This apparent contradiction with the MICs shown in Table 3 indicates possible differences in native substrate and carbapenem uptake or ability to compete for binding, as will be explored later in the article by molecular dynamics modeling. These results are in partial agreement with recent results obtained by Eren et al. (2012), who tested the ability of purified channel-overexpressing membrane vesicles to take up radiolabeled natural substrates in the presence or absence of a variety of antibiotics, and showed that both meropenem and imipenem could compete with arginine uptake by OccD1 as previously described (Trias and Nikaido, 1990; Huang and Hancock, 1993) but neither molecule could compete with arginine uptake by OccD3. In contrast to our results, these authors interpreted their results to mean that OccD3 is incapable of carbapenem transport. It is possible that the results of these studies may differ depending on how the measurements are made to evaluate competition; Eren et al. (2012) measured the effect of excess antibiotic on substrate uptake, whereas in this report the opposite evaluation, i.e. the effect of excess substrate on antibiotic uptake, was made. Alternatively, this discrepancy could be explained by the possibility that sufficient differences exist between the transient binding modes of natural substrates versus carbapenems in OccD3, so that these molecules do not in fact compete directly with each other for transport. We subsequently used computational metadynamics simulations to compare the interactions among the substrates and

Table 3. Whole-Cell Compound Uptake Assay Confirms that OccD1 and OccD3 Both Facilitate Carbapenem Transport, which Is Compromised in a Rationally Designed Meropenem Analog

Omp8 *E. coli* Bearing	MER	Fold Change	IMP	Fold Change	DOR	Fold Change	Compound **7**	Fold Change	CAZ	OX	TO
pB22 (empty)	8	–	4	–	4	–	4	–	1	1	0.016
pB22_OccD1	0.25	↓32×	0.5	↓8×	0.25	↓16×	0.5	↓8×	1	0.5	0.016
pB22_OccD3	0.5	↓16×	0.5	↓8×	0.5	↓8×	0.5	↓8×	0.5	0.5	0.016
pB22_OccK7	8	NC	4	NC	4	NC	4	NC	0.5	0.5	0.016
pB22_OccD2	4	↓2×	2	↓2×	2	↓2×	2	↓2×	0.5	1	0.016

The activity (MIC, in μg/ml) of each test compound against an *E. coli* porin-deficient strain, *omp8*, containing overexpression plasmids as indicated, is shown. Where indicated, fold change is relative to the activity of the *omp8* parent strain with an empty vector. MER, meropenem; IMP, imipenem; DOR, doripenem; CAZ, ceftazidime; TO, tobramycin; OX, ofloxacin. All MIC tests were performed at least in triplicate.

carbapenems with OccD1 and OccD3, both to address this hypothesis and to further define the structural elements that may be involved in carbapenem transport.

Use of Computational Metadynamics Simulations to Define Structural Elements of Carbapenem Transport

Computational metadynamics simulations were employed to better understand how the natural substrates or antibacterial compounds behave in the constriction zone of OccD1 and OccD3.

Two collective variables were selected: the position of the substrate along the long axis of the channel, or its Z coordinate; and a second variable designed to improve sampling within the recognition pocket (Figure S1). The metadynamics biased potentials selected enable enhanced sampling through the channels and result in a two-dimensional projection of the free energy surface. Obtaining accurate free energy profiles/barriers for complex biological processes is notoriously difficult, due to the huge amounts of computer time required to adequately sample all relevant degrees of freedom in a suitable model system. Great strides have been made using specialized hardware (Shaw et al., 2010) and GPU-enabled molecular dynamics codes (Lawrenz et al., 2015) yet in practice these methods are still too costly for routine application, for example, for rank ordering the permeability of a membrane channel to a series of ligands. Metadynamics is one of a number of so-called enhanced sampling techniques developed to reduce the amount of simulation time (and therefore computer time) required to model such processes. Metadynamics works by injecting small amounts of energy into the model system of interest in order to discourage components of the system from repeatedly adopting configurations that have been previously sampled in a simulation; in that way, the method achieves the desired effect of sampling a larger fraction of configurational space in the same overall simulation time. The fact that metadynamics perturbs the system by adding energy can result in sampling nonphysical configurations. For simple systems, this can be avoided by careful choice of the amount of, and frequency with which, energy is added to the system. For large systems with many degrees of freedom, however, it is much more difficult to choose values for these parameters that do not produce nonphysical configurations yet still provide the benefit of enhanced sampling. We found that, in metadynamics simulations of porin/ligand complexes, trajectories that involved nonphysical configurations corresponded to unrealistically high translocation free energies. We therefore adopted the strategy of running numerous (~100) simulations for each porin/ligand complex, monitoring changes in the translocation barrier as a sort of convergence criterion and utilizing only the lowest-energy trajectories when comparing the energetics of different complexes. Furthermore, we found that constraining the porins in the open conformation reduced the frequency of high-energy configurations, gave more rapid convergence, and increased the confidence with which comparisons of the free energy barrier due to the constriction zone could be made. Due to the use of constraints, these calculations probably cannot provide meaningful structural insights into flexible regions of the protein, for example interactions with the loops in the extracellular vestibule, which are additionally confounded by the need to accurately model interactions with lipopolysaccharide molecules in the outer leaflet and which have so far eluded simulation. However, we show that this approach is fit for purpose as a medium-throughput virtual screening platform for the structure-based design of compounds with enhanced porin permeation characteristics.

The minimum free energy profile thus obtained for each system is shown in Figure S2. In order to simplify comparison among systems, the resulting free energy surface obtained from each simulation was normalized by setting to zero the minimum free energy observed for the system configuration with the substrate in the vestibule on the extracellular side of the constriction zone (centered around a Z coordinate value of ~10 Å). The superimposed profiles for OccD1 are shown in Figure S3A. On this profile, the origin (Z coordinate value of 0) corresponds to the center of the channel as defined in the Proteins in Membranes database (Lomize et al., 2006), with the positive axis oriented toward the extracellular space. The substrate recognition pocket is located beyond the center of the channel toward the periplasmic side and corresponds to a Z coordinate value of ~−5 Å. In this pocket, substrates of OccD1 appear to make favorable interactions with Asp 307 and Arg 391 (see Figure 3; Discussion).

The native substrate, arginine, experiences the lowest free energy barrier on translocation through OccD1, and is stabilized in the recognition pocket by ~3 kcal/mol. Imipenem experiences a slightly larger barrier of ~6 kcal, but is similarly stabilized in the recognition pocket by ~4 kcal relative to the vestibular configuration. In the simulations, imipenem closely mimics the electrostatic signature of arginine and makes similar interactions with Asp 307 and Arg 391 (Figure 3B) in the recognition pocket. In contrast, meropenem is not significantly stabilized by interactions in the recognition pocket relative to the vestibule, although

Table 4. Defining Key Residues in Carbapenem Transport Using the Whole-Cell Compound Uptake Assay in the Absence or Presence of the Natural Substrates of OccD1 and OccD3

	Meropenem				Imipenem			
Overexpression Construct	NA	Arginine	Lysine	Gly-Glu	NA	Arginine	Lysine	Gly-Glu
pB22 (empty)	8	8	8	8	4	4	4	4
WT OccD1	0.25	4	4	0.25	0.5	1	1	1
Y176A	2	8	8	2	1	2	2	1
Y282A	0.125	2	2	0.125	0.5	1	1	0.5
Y282R	8	8	4	4	4	2	2	2
D295A	0.25	2	2	0.25	0.5	0.5	1	1
D295H	0.25	2	2	0.25	0.5	0.5	1	1
Y282R, D307H	4	4	4	4	2	1	2	2
D307A	0.25	0.25	0.25	0.125	0.5	0.5	0.5	0.5
D307H	4	4	4	4	2	1	2	2
R389A	1	4	4	1	1	1	2	1
R391A	1	4	4	0.5	1	1	2	1
R410A	2	4	4	2	1	1	2	1
WT OccD3	0.5	0.5	0.5	0.5	0.5	0.5	0.5	0.5
Y326A	0.5	0.5	0.5	0.5	0.5	0.5	0.5	0.5
Y326R	0.5	0.5	0.5	0.5	0.5	0.5	0.5	1
D342A	0.5	0.5	0.5	0.5	0.5	0.5	0.5	0.5
D342H	1	1	1	1	1	1	1	1

The activity (MIC, in μg/ml) of either meropenem or imipenem against an *E. coli* porin-deficient strain, *omp8*, overexpressing either wild-type or mutant OccD1, in the presence of 50 mM arginine, lysine or Gly-Glu, is shown. NA, no amino acid added. All MIC tests were performed at least in triplicate.

it exhibits a similar barrier to imipenem. In the Y282R/D307H double mutant, which introduces unfavorable interactions in the recognition pocket, the barrier to translocation of imipenem rises to ~12 kcal/mol and the relative stabilization in the recognition pocket is lost. The barrier for meropenem is indeterminate as meropenem was not observed to enter the recognition pocket or even sample configurations beyond the center of the channel in any of the simulations run with this double mutant. Qualitatively, the energy barriers and relative stabilization in the recognition pocket of imipenem and meropenem in wild-type and mutant OccD1 are consistent with the observed trends in cellular activity.

Amino Acid Substitutions Reveal Important Differences in Substrate versus Carbapenem Transport

To further characterize the contribution of key channel residues shown to interact with natural substrates and their effect on the ability to transport carbapenems in OccD1 and OccD3, we generated a number of point mutants based both on the molecular modeling results described above and on previous work by the van den Berg laboratory. These researchers evaluated the effect of a number of amino acid substitutions at predicted natural substrate transient binding residues of OccD1 and analyzed their ability to transport arginine (Eren et al., 2013). They found that replacing conserved residues Arg389, Arg391, and Arg410 within the basic ladder and Asp307 within the recognition pocket (Figure 2) with alanine resulted in the biggest effect on arginine uptake. Reversing the charge of the recognition pocket residues by converting Tyr176, Tyr282, or Asp307 to arginine or histidine had little effect when the mutants were tested individually, however, the double mutant Tyr282Arg/Asp307His and the triple mutant Tyr176Arg/Tyr282Arg/Asp307His both showed major deficiencies in arginine transport (Eren et al., 2013). Accordingly, we generated several of these mutations and tested them in our cell-based compound uptake assay with and without competition by excess natural substrate (Table 4). Within the recognition pocket, we found that changing Tyr176 to alanine resulted in an MIC shift from 0.25 to 2 μg/ml for meropenem and 0.5 to 1 μg/ml for imipenem, i.e. it reduced but did not abolish the level of carbapenem uptake, and addition of Arg or Lys (but not Gly-Glu) to the culture medium rendered the channel inactive for meropenem, suggesting competition still occurred in the presence of this mutation. In contrast, a Tyr282Ala mutant had no effect on MICs, i.e. showed wild-type levels of carbapenem uptake and active competition with Arg or Lys but a Tyr282Arg mutant had the same MIC as empty vector, suggesting it is incapable of transporting carbapenems. Although mutation of Asp307 to Ala reduced arginine uptake according to Eren et al. (2012), we found this change had no effect on carbapenem uptake by OccD1. Of particular interest is the fact that this mutation appeared to abrogate competition with natural substrates as their addition had no effect on carbapenem susceptibility. In contrast, changing Asp307 to a histidine had a significant effect on carbapenem transport, whereas this mutation had no effect on arginine transport according to Eren et al. (2012). Not surprisingly, the double mutant Tyr292Arg/Asp307His is equally ineffective in carbapenem transport as either mutant tested alone (Table 4). We then tested several mutations within the basic ladder; Arg389Ala, Arg391Ala, and Arg410Ala mutants all showed a reduction but not complete loss of carbapenem transport (with

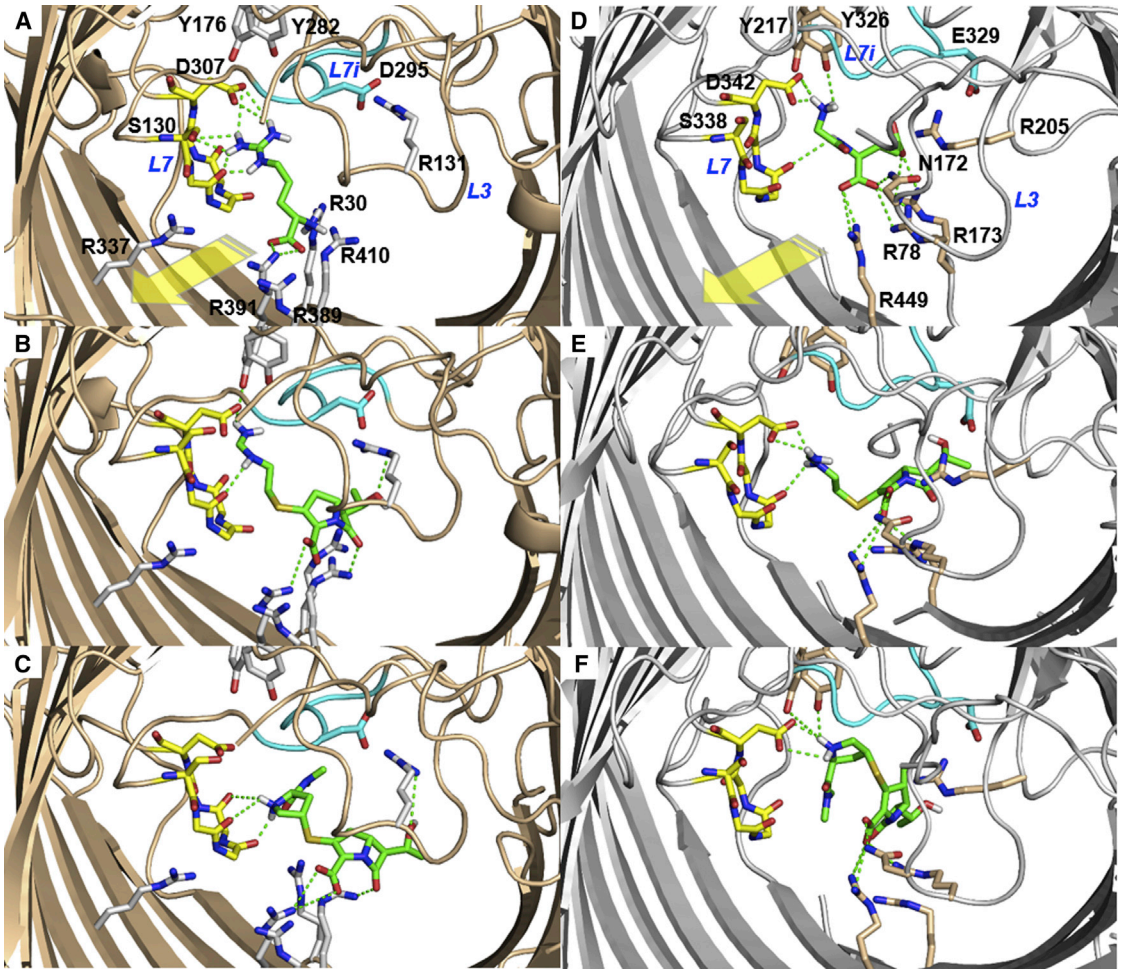

Figure 3. Modeled Interactions with the Recognition Pocket

All channels were aligned using the protein structure alignment tool in Schrodinger.

(A) Arginine with OccD1.

(B) Imipenem with OccD1.

(C) Meropenem with OccD1.

(D) Glycine-glutamate with OccD3.

(E) Imipenem with OccD3.

(F) Meropenem with OccD3.

Arrows represent the extracellular to periplasmic space direction.

2- to 4-fold shifts in MIC compared with wild-type OccD1) and all showed competition with Arg or Lys. Overall, these results suggest that the mode of transient binding of carbapenems to OccD1, although similar, is not identical to the transient binding of natural substrates arginine and lysine. Similarly, we evaluated the effect of altering two key residues within the predicted recognition pocket of OccD3 Tyr326 and Asp342 (Figure 2C). Changing either of these to either Ala/Arg or Ala/His, respectively, had no effect on carbapenem MICs compared with wild-type OccD3, suggesting that neither affected its recognition or transient binding of these molecules. Addition of excess Gly-Glu also had no effect. These results support the conclusion generated by modeling and metadynamics simulations described above, namely that the mode of carbapenem transport by OccD3 differs in several important ways from that of OccD1.

Carbapenem Analogs with Altered Uptake Properties

In order to facilitate the rational design of carbapenems with altered uptake properties, we focused our attention on the side-chain derivatives of these carbapenems recognizing that several features of the core molecule are required for PBP binding (e.g. the activating group carboxylate, hydroxylethyl group). Compound **7** (Figure 1) was designed to explore the importance of the dimethyl amide moiety in meropenem and explore the effect of adding an additional negative charge to the molecule. Interestingly, while compound **7** does lose some cellular activity, its dependence on OccD1 as a major route of permeation appears significantly diminished with MICs of 4–8 μg/ml across wild-type and channel-deficient strains (Table 2) and much less activity in the OccD1 overexpressing *E. coli* strain compared with meropenem (Table 3). Similarly, compound **8** (Figure 1)

(Eguchi et al., 2007; Kanazawa et al., 1999) was synthesized as an analog, which could abolish the favorable interactions that imipenem makes with Asp307 in the recognition pocket and thus remove specificity for OccD1 and potentially enable enhanced permeation through OccD3. Notably, the barrier to translocation in the simulations for compound **8** rose beyond 20 kcal/mol (Figure S3B), further supporting the importance of favorable interactions with Asp 307 in the recognition pocket. This resulted in complete lack of cellular activity of compound **8** while the potency on the PBP3 target actually improved 5-fold (Table S3).

In OccD3, there is effectively no barrier to translocation for the native substrate, Gly-Glu (see Figure S3B). The privileged carbapenems imipenem and meropenem also exhibit modest barriers, consistent with a role for OccD3 in the uptake of these antibiotics. Neither drug binds deeply in the Gly-Glu recognition pocket, mostly likely due to its being in a more open state (Figure 2C). This suggests that further optimization of these compounds may be possible in order to increase permeability and reduce susceptibility to OccD1-mediated carbapenem resistance.

DISCUSSION

The success rate in the identification of novel antibacterial agents to treat Gram-negative infections is insufficient; indeed, an agent acting via a novel mechanism of action has not been discovered in nearly half a century. In order to address this medical need, novel approaches to this very challenging problem must be undertaken immediately. Typically, drug discovery programs aimed at the design of novel Gram-negative agents use cell-based susceptibility assays on wild-type or permeabilized strains. While this type of assay can provide meaningful information for chemical series that exhibit whole-cell killing activities, it is a rather blunt toolset when the goal is to design better permeation into a series that inhibits an essential target but suffers from poor permeability. The work described here illustrates our early attempts to build a multidisciplinary approach to this challenge by incorporating: (1) methods to identify channels involved in permeation for novel compounds, (2) genetically altered cell-based systems to probe the relevance of these channels, (3) molecular simulation to identify key residues involved in recognition, which can be tested in the genetically altered cell systems, and, ultimately, (4) application of the structural information obtained from these methods in the design of analogs to test and confirm these hypotheses. This new toolkit should provide us with information about cell permeation in a much more focused manner than has been demonstrated previously and thus eventually allow the design of novel antibacterials with much more resolution than is provided by the traditional blunt tools that have historically driven drug discovery in this area.

While the results described herein are preliminary, their significance illustrates the great promise of this approach. Using the TNseq platform, we have discovered a second mode of permeation for meropenem in OccD3. Our modeling work on this channel was based on its solved crystal structure and its further exploration will be communicated in due course. Our work on OccD1 led to the design of compound **7**, a meropenem analog that appears to permeate with much less dependence on OccD1 yet still exhibits antibacterial activity. Another interesting result highlighted in this work is our finding that *N*-acetyl thienamycin (compound **8**), an imipenem analog devoid of the positive charge provided by the amidine moiety is inactive in cells due to issues of permeability, as its acylation rate of PBP3 is actually enhanced compared with that of imipenem. Our modeling efforts have identified further key residues that are involved in the structural recognition of OccD1 and further efforts are underway to use these data to design analogs that take advantage of these interactions. This finding is in agreement with work from Lou et al. (2011) who found that subtle changes in the constriction zone of *E. coli* OmpC appears to affect antibiotic uptake while maintaining suitable nutrient uptake.

While we are not yet close to solving this important problem, these efforts may pave the way for a new approach to understanding Gram-negative permeation, which we hope will ultimately lead to novel antibacterials in this much needed area.

SIGNIFICANCE

One of the biggest challenges in the design and development of new drugs for the treatment of infections caused by *P. aeruginosa* and other serious Gram-negative pathogens is our relative ignorance of the molecular mechanisms driving compound penetration across their outer membranes. Definition of these mechanisms is considered to be essential for significant advances in the ability to rationally design antimicrobial compounds, yet they still remain poorly understood. This challenging problem was assessed through the implementation of a multidisciplinary approach, namely genetics, molecular dynamics simulations, and medicinal chemistry to first identify uptake determinants, followed by analysis of uptake on an atomic scale, and ultimately, the rational design and synthesis of novel antibiotic analogs with altered uptake properties. Saturated transposon libraries were subjected to treatment with meropenem and analyzed by TNseq. Results not only confirmed the well-established role of OccD1/OprD in meropenem uptake but also identified a previously unknown second mode of transport via the channel OccD3/OpdP. Carbapenem passage through these channels was confirmed with a novel cell-based assay, and further defined at the atomic level using computational metadynamics simulations. These results were then used to rationally design carbapenem analogs, which demonstrated the predicted alteration in channel transmissibility. This report demonstrates the potential for the rational design of bacterial compound uptake. These findings also lay the groundwork for the deployment of a platform that may be applicable for investigating the uptake of potentially any class of antibacterial compounds.

EXPERIMENTAL PROCEDURES

Growth of Bacterial Strains

Strains of *P. aeruginosa* were grown in Luria-Bertani agar (BD cat. no. 244510), MHBII (BD cat. no. 297311), or M9 minimal medium (BD cat. no. 248510) containing 30 mM sodium succinate as a carbon source (M9S). Gentamicin was used at 30 μg/ml where appropriate. For plasmid maintenance during mutant construction in *P. aeruginosa,* the medium was supplemented with 200 μg/ml of carbenicillin and 100 μg/ml of tetracycline. Strains of *E. coli* were grown in

LB or M9 minimal medium containing 0.2% glucose as a carbon source (M9G). Ampicillin or gentamicin were used at 100 μg/ml or 12 μg/ml, respectively, where appropriate.

Construction of Mutant and Overexpression Strains in PAO1 and *E. coli* Omp8

PCR products of the 533-bp upstream and 544-bp downstream regions of the *occD1/oprD* (*PA4501*) open reading frame (ORF) in PA01 were fused by splice overlap extension PCR to flank a third PCR product consisting of a gentamicin resistance gene (*aacC1*) along with the Flp recombinase target (FRT) sites on either side of the gene, resulting in a final fragment of 2073 bp which was cloned into TOPO vector (TOPO TA Cloning Kit K4500-01 from Invitrogen). The TOPO cloning reaction was transformed into *E. coli* TOP10 cells (C4040-10, Invitrogen). Positive clones, which were selected on LB agar containing 30 μg/ml, were screened by colony PCR. The desired sequence in the positive clone, pAN134, was confirmed by Sanger sequencing. Plasmid pAN134, which behaves as a suicide vector in *P. aeruginosa*, was then electroporated into PA01 containing pAN131 (a derivative of pUCP18 that contains λRed genes (αβδ) whose expression is controlled by the arabinose-inducible pBAD promoter as well as the counter-selectable marker *sacB*) as described in Lesic and Rahme (2008). Positive clones (where the ORF of *occD1* was replaced by *aacC1*) were selected on LB supplemented with 15 μg/ml gentamicin, then cured of pAN131 by counterselection of colonies that survived overnight growth on LB agar containing10% sucrose. The insertion of the *aacC1* gene in the ORF of *occD1* was confirmed by PCR followed by Sanger sequencing. This gentamicin resistance marker was excised by electroporating a pFLP3 plasmid (Choi et al., 2005) that expresses the Flp recombinase, which induces recombination at the engineered FRT sites, resulting in an unmarked deletion of *occD1*. Finally, the pFLP3 plasmid was cured from Δ*oprD* strain by sucrose selection as described above. The clean *occD1* deletion was confirmed by next-generation sequencing (Illumina MiSeq) of total genomic DNA purified from the strain. PAO1 Δ*occD3/opdP* and the five-channel knockout strain (*ΔoprD/occD1*, *ΔopdC/occD2 ΔOpdP/occD3*, *ΔopdT/occD4 ΔopdB/occD7*) were constructed by Microbiotix. The unmarked double deletion mutant PAO1 Δ*occD1*Δ*occD3* was engineered following the same protocol used for constructing Δ*occD1* using Δ*occD3* as the parent strain.

For construction of channel overexpression vectors for *P. aeruginosa*, channel genes were amplified with iProof High-Fidelity DNA polymerase with primers containing SacI (5′ end) or BamHI (3′ end) restriction sites (Bio-Rad). Fragments were ligated to SacI/BamHI (New England Biolabs) digested *E. coli/P. aeruginosa* shuttle vector pPSV35 (Rietsch et al., 2005). Ligations were used to transform *E. coli* Top 10 strain (Life Technologies) with selection on gentamycin. Clones were selected and the presence of the channel insert was confirmed by sequencing and restriction analysis. Plasmid was recovered and used to transform PAO1 strains. For construction of pseudomonal channel overexpression vectors in *E. coli*, plasmid pB22, which contains an N-terminal *E. coli* outer membrane protein signal sequence (Eren et al., 2012), was amplified with inverse primers, with the upstream reverse primer containing a 5′ phosphate and the 3′ forward primer including the pB22 XbaI site. Channel genes were amplified with upstream primers containing a 5′ phosphate and 3′ primers at the XbaI site. PCR products were digested with XbaI, ligated (Express Link; Life Technologies) and used to transform *E. coli* Omp8. Inverse PCR was used to create amino acid mutations within channel genes. Mutations were made in overlapping primers oriented in opposite directions to amplify the entire pB22 plasmid containing wild-type *OccD1* or *OccD3.* DpnI was used for the digestion of parental DNA from the PCR reaction, followed by transformation of *E. coli* Omp8 cells (Table S4). All primer sequences are available upon request.

MIC Determination in *P. aeruginosa*

For MIC determination in PAO1 strains, overnight stationary cultures were diluted 1:10,000 and used to inoculate MIC plates (Corning 3799) containing test antibiotics. Final concentrations of isopropyl β-D-1-thiogalactopyranoside (Invitrogen) at 100 μM and gentamicin at 30 μg/ml were used where appropriate. All strains were grown in MHBII or M9S.

Construction of Transposon Mutant Libraries in PAO1

Plasmid pAZ200, which contains a TN5 derivative with a tetracycline resistance cassette between the transposon mosaic ends and a transposase and genes necessary for conjugal transfer outside of the mosaic ends, was used to transform *E. coli* mating strain SM10. Donor *E. coli* and recipient *P. aeruginosa* strains were grown in 20-ml cultures overnight in LB. *P. aeruginosa* cultures were heat shocked for 1 hr at 42°C. Donor and recipient cultures were mixed in a 1:1 ratio and centrifuged for 10 min at 5,000 × g. Cell pellets were resuspended in 250 μl of LB containing 1 mM $MgCl_2$, spotted onto 47-mm Nuclepore polycarbonate track-etch membranes (Whatman), and incubated at 37°C for 5 hr. Filters were resuspended in 5 ml of LB and the entire suspension was spread over 150-mm diameter petri plates containing LB with tetracycline at 60 μg/ml and chloramphenicol at 10 μg/ml to counterselect against *E. coli*. After 2 days of incubation at 37°C, the resulting resistant colonies were scraped and pooled in LB, and aliquots were frozen for storage.

Antibiotic Treatment of Pooled TN Libraries

Approximately 5 × 10^6 cfu from pooled TN mutant libraries were used to inoculate 10 ml of LB containing meropenem at the MIC. For TNseq input and output samples, 100-μl aliquots were removed from cultures before and after drug treatment, resuspended in fresh LB, and spread over multiple 150-mm petri plates. To prevent overgrowth and overrepresentation of fast-growing mutants, plates were incubated for 14 hr at 30°C. Colonies were scraped, pooled, pelleted, and used for preparation of TNseq genomic libraries.

Preparation of TNseq Genomic Libraries

TNseq libraries were prepared based on the protocol from the Camilli laboratory (van Opijnen et al., 2014). Please see the Supplemental Information for a detailed explanation of the method employed in the generation, sequencing, and analysis of TNseq libraries.

Whole-Cell Compound Uptake Assay

E. coli Omp8 strains harboring plasmids with arabinose-inducible pseudomonal channels were grown overnight in M9G containing ampicillin. Overnight cultures were diluted 1:50 in fresh M9G and grown shaking for 5 hr at 37°, at which point L-arabinose (Sigma) was added at 0.0125% and cells were allowed to induce channel expression for 3 hr. Cells were diluted 1:100 into fresh M9G and 100-μl aliquots were used to inoculate the wells of 96-well round-bottom plates (Corning 3799) containing test antibiotics, ampicillin (final concentration 100 μg/ml), and L-arabinose (final concentration 0.0125%). A tetrazolium salt solution containing WST-8 (Sigma; CCK-8) was used at a final concentration of 2% to aid in visualization of cell growth.

Metadynamics Simulations of OccD1 and OccD3

All simulations were performed using Desmond (Bowers et al., 2006) and the Schrödinger suite of modeling tools (Schrödinger, 2014). X-Ray crystal structures were used as starting points for simulations on OccD1 and OccD3 (Eren et al., 2012) (PDB IDs 3SY7 and 3SYB, respectively). Please see Supplemental Information for a detailed description of the methods employed.

Carbapenem Synthesis

The experimental methods for the synthesis of compounds **7** and **8** can be found in the Supplemental Information.

SUPPLEMENTAL INFORMATION

Supplemental Information includes Supplemental Experimental Procedures, three figures, and four tables and can be found with this article online at http://dx.doi.org/10.1016/j.chembiol.2015.03.018.

AUTHOR CONTRIBUTIONS

V.M.I. and A.J.C. performed the genetic and computational modeling experiments, respectively. M.S. designed novel carbapenem analogs, A.N. provided bacterial reagents, K.E.F. conducted the MIC assays. V.M.I., A.J.C., J.M., R.T., and A.A.M. analyzed the data and wrote the paper.

ACKNOWLEDGMENTS

The authors thank Bert van den Berg for his gift of the *E. coli* Omp8 strain and pB22 plasmid, Victoria Korboukh for her help in early uptake assay

development, Bob McLaughlin for his help with TNseq, and Paul Miller for his invaluable leadership and support. They also would like to acknowledge chemists at Pharmaron for their efforts in preparing an intermediate for these studies and the Schrödinger group of scientists for valuable discussions on Desmond and metadynamics. The research leading to these results was conducted as part of the Translocation Consortium (www.translocation.eu) and has received support from the Innovative Medicines Joint Undertaking under Grant Agreement no. 115525, resources which are composed of financial contribution from the European Union's Seventh Framework Programme (FP7/2007-2013) and in-kind contributions from EFPIA companies. All authors are current or former employees of AstraZeneca and, as such, may hold stock in the company.

Received: December 29, 2014
Revised: March 14, 2015
Accepted: March 27, 2015
Published: April 23, 2015

REFERENCES

Biswas, S., Mohammad, M.M., Patel, D.R., Movileanu, L., and van den Berg, B. (2007). Structural insight into OprD substrate specificity. Nat. Struct. Mol. Biol. *14*, 1108–1109.

Bowers, K.J., Chow, E., Xu, H., Dror, R.O., Eastwood, M.P., Gregersen, B.A., Klepeis, J.L., Kolossvary, I., Moraes, M.A., Sacerdoti, F.D., et al. (2006). Scalable algorithms for molecular dynamics simulations on commodity clusters. In Proceedings of the 2006 ACM/IEEE Conference on Supercomputing (ACM), p. 84.

Breidenstein, E.B.M., de la Fuente-Núñez, C., and Hancock, R.E.W. (2011). *Pseudomonas aeruginosa*: all roads lead to resistance. Trends Microbiol. *19*, 419–426.

Choi, K.-H., Gaynor, J.B., White, K.G., Lopez, C., Bosio, C.M., Karkhoff-Schweizer, R.R., and Schweizer, H.P. (2005). A Tn7-based broad-range bacterial cloning and expression system. Nat. Methods *2*, 443–448.

Eguchi, K., Ueda, Y., Kanazawa, K., Sunagawa, M., and Gotoh, N. (2007). The mode of action of 2-(thiazol-2-ylthio)-1beta-methylcarbapenems against *Pseudomonas aeruginosa*: the impact of outer membrane permeability and the contribution of MexAB-OprM efflux system. J. Antibiot. (Tokyo) *60*, 129–135.

Eren, E., Vijayaraghavan, J., Liu, J., Cheneke, B.R., Touw, D.S., Lepore, B.W., Indic, M., Movileanu, L., and van den Berg, B. (2012). Substrate specificity within a family of outer membrane carboxylate channels. PLoS Biol. *10*, e1001242.

Eren, E., Parkin, J., Adelanwa, A., Cheneke, B., Movileanu, L., Khalid, S., and van den Berg, B. (2013). Toward understanding the outer membrane uptake of small molecules by *Pseudomonas aeruginosa*. J. Biol. Chem. *288*, 12042–12053.

Fraimow, H., and Nahra, R. (2013). Resistant gram-negative infections. Crit. Care Clin. *29*, 895–921.

Hajjar, E., Bessonov, A., Molitor, A., Kumar, A., Mahendran, K.R., Winterhalter, M., Pagès, J.-M., Ruggerone, P., and Ceccarelli, M. (2010). Toward screening for antibiotics with enhanced permeation properties through bacterial porins. Biochemistry *49*, 6928–6935.

Hancock, R.A., and Woodruff, W.A. (1988). Roles of porin and beta-lactamase in beta-lactam resistance of *Pseudomonas aeruginosa*. Rev. Infect. Dis. *10*, 770–775.

Hancock, R.E., and Brinkman, F.S. (2002). Function of pseudomonas porins in uptake and efflux. Annu. Rev. Microbiol. *56*, 17–38.

Hombach, M., Bloemberg, G.V., and Böttger, E.C. (2012). Effects of clinical breakpoint changes in CLSI guidelines 2010/2011 and EUCAST guidelines 2011 on antibiotic susceptibility test reporting of Gram-negative bacilli. J. Antimicrob. Chemother. *67*, 622–632.

Huang, H., and Hancock, R.E. (1993). Genetic definition of the substrate selectivity of outer membrane porin protein OprD of *Pseudomonas aeruginosa*. J. Bacteriol. *175*, 7793–7800.

Kanazawa, K., Nouda, H., Sumita, Y., and Sunagawa, M. (1999). Structure-activity relationships of carbapenems to the antagonism of the antipseudomonal activity of other beta-lactam agents and to the beta-lactamase inducibility in *Pseudomonas aeruginosa*: effects of 1beta-methyl group and C-2 side chain. J. Antibiot. (Tokyo) *52*, 142–149.

Köhler, T., Michea-Hamzehpour, M., Epp, S.F., and Pechere, J.-C. (1999). Carbapenem activities against *Pseudomonas aeruginosa*: respective contributions of OprD and efflux systems. Antimicrob. Agents Chemother. *43*, 424–427.

Kumar, A., Hajjar, E., Ruggerone, P., and Ceccarelli, M. (2010). Molecular simulations reveal the mechanism and the determinants for ampicillin translocation through OmpF. J. Phys. Chem. B *114*, 9608–9616.

Laio, A., and Parrinello, M. (2002). Escaping free-energy minima. Proc. Natl. Acad. Sci. USA *99*, 12562–12566.

Lawrenz, M., Shukla, D., and Pande, V.S. (2015). Cloud computing approaches for prediction of ligand binding poses and pathways. Sci. Rep. *5*, 7918.

Lesic, B., and Rahme, L. (2008). Use of the lambda Red recombinase system to rapidly generate mutants in *Pseudomonas aeruginosa*. BMC Mol. Biol. *9*, 20.

Liu, J., Eren, E., Vijayaraghavan, J., Cheneke, B.R., Indic, M., van den Berg, B., and Movileanu, L. (2012a). OccK channels from *Pseudomonas aeruginosa* exhibit diverse single-channel electrical signatures but conserved anion selectivity. Biochemistry *51*, 2319–2330.

Liu, J., Wolfe, A.J., Eren, E., Vijayaraghavan, J., Indic, M., van den Berg, B., and Movileanu, L. (2012b). Cation selectivity is a conserved feature in the OccD subfamily of *Pseudomonas aeruginosa*. Biochim. Biophys. Acta *1818*, 2908–2916.

Lomize, M.A., Lomize, A.L., Pogozheva, I.D., and Mosberg, H.I. (2006). OPM: Orientations of Proteins in Membranes database. Bioinformatics *22*, 623–625.

Lou, H., Chen, M., Black, S.S., Bushell, S.R., Ceccarelli, M., Mach, T., Beis, K., Low, A.S., Bamford, V.A., Booth, I.R., et al. (2011). Altered antibiotic transport in OmpC mutants isolated from a series of clinical strains of multi-drug resistant *E. coli*. PLoS One *6*, e25825.

Moya, B., Dötsch, A., Juan, C., Blázquez, J., Zamorano, L., Haussler, S., and Oliver, A. (2009). β-Lactam resistance response triggered by inactivation of a nonessential penicillin-binding protein. PLoS Pathog. *5*, e1000353.

Palace, S.G., Proulx, M.K., Lu, S., Baker, R.E., and Goguen, J.D. (2014). Genome-wide mutant fitness profiling identifies nutritional requirements for optimal growth of *Yersinia pestis* in deep tissue. MBio *5*, e01385–14.

Papp-Wallace, K.M., Endimiani, A., Taracila, M.A., and Bonomo, R.A. (2011). Carbapenems: past, present, and future. Antimicrob. Agents Chemother. *55*, 4943–4960.

Parkin, J., and Khalid, S. (2014). Atomistic molecular-dynamics simulations enable prediction of the arginine permeation pathway through OccD1/OprD from *Pseudomonas aeruginosa*. Biophys. J. *107*, 1853–1861.

Pendleton, J.N., Gorman, S.P., and Gilmore, B.F. (2013). Clinical relevance of the ESKAPE pathogens. Expert Rev. Anti Infect. Ther. *11*, 297–308.

Pirnay, J.-P., Vos, D.D., Mossialos, D., Vanderkelen, A., Cornelis, P., and Zizi, M. (2002). Analysis of the *Pseudomonas aeruginosa* oprD gene from clinical and environmental isolates. Environ. Microbiol. *4*, 872–882.

Prilipov, A., Phale, P.S., Van Gelder, P., Rosenbusch, J.P., and Koebnik, R. (1998). Coupling site-directed mutagenesis with high-level expression: large scale production of mutant porins from *E. coli*. FEMS Microbiol. Lett. *163*, 65–72.

Quale, J., Bratu, S., Gupta, J., and Landman, D. (2006). Interplay of efflux system, *ampC*, and *oprD* expression in carbapenem resistance of *Pseudomonas aeruginosa* clinical isolates. Antimicrob. Agents Chemother. *50*, 1633–1641.

Quinn, J.P., Dudek, E.J., DiVincenzo, C.A., Lucks, D.A., and Lerner, S.A. (1986). Emergence of resistance to imipenem during therapy for *Pseudomonas aeruginosa* infections. J. Infect. Dis. *154*, 289–294.

Rietsch, A., Vallet-Gely, I., Dove, S.L., and Mekalanos, J.J. (2005). ExsE, a secreted regulator of type III secretion genes in *Pseudomonas aeruginosa*. Proc. Natl. Acad. Sci. USA *102*, 8006–8011.

Schrödinger. (2014). Schrödinger Release 2014-1: Maestro, Version 9.7. (Schrödinger LLC).

Shaw, D.E., Maragakis, P., Lindorff-Larsen, K., Piana, S., Dror, R.O., Eastwood, M.P., Bank, J.A., Jumper, J.M., Salmon, J.K., Shan, Y., and Wriggers, W. (2010). Atomic-level characterization of the structural dynamics of proteins. Science *330*, 341–346.

Skurnik, D., Roux, D., Cattoir, V., Danilchanka, O., Lu, X., Yoder-Himes, D.R., Han, K., Guillard, T., Jiang, D., Gaultier, C., et al. (2013). Enhanced in vivo fitness of carbapenem-resistant *oprD* mutants of *Pseudomonas aeruginosa* revealed through high-throughput sequencing. Proc. Natl. Acad. Sci. USA *110*, 20747–20752.

Sobel, M.L., Hocquet, D., Cao, L., Plesiat, P., and Poole, K. (2005). Mutations in PA3574 (nalD) lead to increased MexAB-OprM expression and multidrug resistance in laboratory and clinical isolates of *Pseudomonas aeruginosa*. Antimicrob. Agents Chemother. *49*, 1782–1786.

Subashchandrabose, S., Smith, S.N., Spurbeck, R.R., Kole, M.M., and Mobley, H.L.T. (2013). Genome-wide detection of fitness genes in uropathogenic *Escherichia coli* during systemic infection. PLoS Pathog. *9*, e1003788.

Tamber, S., and Hancock, R.E.W. (2006). Involvement of two related porins, OprD and OpdP, in the uptake of arginine by *Pseudomonas aeruginosa*. FEMS Microbiol. Lett. *260*, 23–29.

Tamber, S., Ochs, M.M., and Hancock, R.E. (2006). Role of the novel OprD family of porins in nutrient uptake in *Pseudomonas aeruginosa*. J. Bacteriol. *188*, 45–54.

Trias, J., and Nikaido, H. (1990). Protein D2 channel of the *Pseudomonas aeruginosa* outer membrane has a binding site for basic amino acids and peptides. J. Biol. Chem. *265*, 15680–15684.

van Opijnen, T., Lazinski, D.W., and Camilli, A. (2014). Genome-wide fitness and genetic interactions determined by Tn-seq, a high-throughput massively parallel sequencing method for microorganisms. Curr. Protoc. Mol. Biol. *106*, 7.16.1–7.16.24.

Wang, N., Ozer, E.A., Mandel, M.J., and Hauser, A.R. (2014). Genome-wide identification of *Acinetobacter baumannii* genes necessary for persistence in the lung. MBio *5*, e01163–14.